Int J Adv Manuf Technol (2018) 94:1021–1030
DOI 10.1007/s00170-017-0961-2

ORIGINAL ARTICLE

Microstructure characterization and mechanical behavior of dissimilar friction stir welded Al/Cu couple with different joint configurations

Wei Zhang[1] · **Yifu Shen**[1] · **Yinfei Yan**[1] · **Rui Guo**[1] · **Wei Guan**[1] · **Guolin Guo**[1,2]

Received: 23 March 2017 / Accepted: 14 August 2017 / Published online: 24 August 2017

Abstract In the present study, a new tooth-shaped joint configuration (TJC) was adopted to bond Al/Cu dissimilar metals via friction stir welding. TJC is a special joint design to tailor the content of base materials in the weld, aiming to enhance material mixing and flow. For comparison, routine butting joint configuration (BJC) was also conducted under the same process condition. The optimal welding parameters were determined by the trials, including rotational speed 1500 rpm, welding speed 30 mm/min, and plunge depth −0.2 mm. Cross-section microstructure of the joint and interface evolution were investigated utilizing scanning electron microscopy (SEM) equipped with energy dispersive spectrum (EDS). X-ray diffraction (XRD) was applied to characterize the phase composition. Microstructure analysis indicated TJC yielded the defect-free weld and the stir zone could be regarded as the mix of Al matrix and dense particles, which formed the composite structure. Commonly, ultra-thin diffusion layer was developed through the Al/Cu interface for both the joints and EDS results confirmed that the interface is composed of two sublayers for each joint. Then, Cu_2Al and Cu_9Al_4 with low activated energy were formed due to the chemical affinity between Al and Cu. Joint performance was evaluated via tensile test and failure load of the joint fabricated via TJC reached to 9.6 kN, while the corresponding value was 7.9 kN under BJC, suggesting TJC could enhance the joint quality effectively. Besides, fracture mode was transformed from ductility to brittleness under TJC and BJC separately. Fractographic features of the broken specimens were addressed and discussed carefully.

Keywords Friction stir welding · New-typed joint design · Comparative study · Microstructure and performance

1 Introduction

Nowadays, one great need is the application of hybrid components especially in the exceptional industries such as aerospace and defense sectors to satisfy special requirements and give full play to the respective advantages of dissimilar material [1–5]. The very different properties of base materials, however, still pose a challenge for the joining [6]. With time going by, solid state joining techniques appeal to researchers because of the low processing temperature. Friction stir welding (FSW), introduced by The Welding Institute (TWI) in 1991 [7, 8], has been used widely. During the welding, a rotating tool provides the continual hot working action, which will not cause the melting of the base material. FSW reveals its dominance to other methods in fabricating dissimilar metals gradually, thanks to the low distortion and reduced defects, for instance Al to Mg [9–11] and Al to steel [12–14], for the purpose of weight reduction and cost saving.

Al/Cu dissimilar joint could be applied in a variety of sectors due to the high electrical conductivity and good corrosion resistance. Moreover, Al/Cu joint could substitute Cu/Cu joint to save scarce Cu resources [15]. In practice, butt welding takes the priority of selection especially under the circumstance of alternative load, corrosive medium, and extreme temperature, so that a constant effort has been in progress to improve the joint quality and well meet the needs. Some experience related

✉ Yifu Shen
yfshen_nuaa@hotmail.com

[1] College of Materials Science and Technology, Nanjing University of Aeronautics and Astronautics (NUAA), Yudao Street 29, Nanjing 210016, People's Republic of China

[2] School of Automotive and Engineering, Changshu Institute of Technology, Hushan Road 99, Changshu 215500, People's Republic of China

to Al/Cu friction stir butt welding has been drawn during the long-term practice. Generally speaking, Cu with high plasticized temperature is placed at the advancing side (AS) where the tangential velocity is identical to the translation motion of the tool, while Al plate is placed at the other side, namely, retreating side (RS) where the rotation direction of the tool and its traverse direction are consistent. This placement was confirmed by Sahu et al. [16], and they found the joint with high performance could be obtained while placing Cu plate on AS. Similarly, Galvão et al. [17] also stated that putting Al plate at AS leads to the poor welding appearance accompanied by excessive flash and thinness. It is worthy of note that the temperature distribution and material flow are distinctly different at AS and RS, respectively. To yield reliable bonding, offsetting the pin towards Al side is a common method to fill the room induced by the forward motion of the tool because plasticized aluminum possesses good fluidity [18, 19] and meanwhile optimizing process parameters for further improvement of the weld quality. The pin offset is the distance from the axis of pin to the butt line. Al-Roubaiy et al. [20] obtained sound weld with typical Al/Cu FSW characteristics by offsetting the pin towards Al plate assisted with a finite element analysis theoretically. Liu et al. [21] conducted the Al/Cu butt welding with various parameters and they pointed out placing Cu plate at AS without offsetting could achieve the satisfying weld morphology. A study of Al to Cu butt welding was also performed with the assistance of various preheating temperatures and cooling rates by Mehta et al. [22], and they systematically elaborated the influence of each set of parameter, concluding that water cooling could significantly enhance the tensile strength of the joint via inhibiting the development of intermetallics.

FSW could be treated as an in situ extruding process [23], and on the back of the pin, plasticized materials are transported from RS to AS, forming dense weld seam. Consequently, proper material mixing and flow are necessary to fill the squeezed room fully and produce good metallurgical adhesion. Different from the similar material welding, the disproportional mixing of deformed material should be taken into consideration owing to the heterogeneous flow characteristic of dissimilar materials. There is no doubt that placing the pin mostly on Al side with the help of proper welding parameters is a feasible method to achieve reliable bonding as aforementioned. Nevertheless, in terms of the offsetting distance, universally accepted standard has not been reached so far. Besides, different physical characteristic of base metals will hinder the free material flow. In the present work, an original tooth-shaped joint configuration (TJC) was introduced to increase the contact area of base materials and enhance material mixing. According to the practical condition, the composition of the weld could also be adjusted by changing the tooth size, and recently, the authors have confirmed the feasibility of fabricating Al/Cu joint via this special joint form [24]. Figure 1 shows the schematic diagram of the FSW setup.

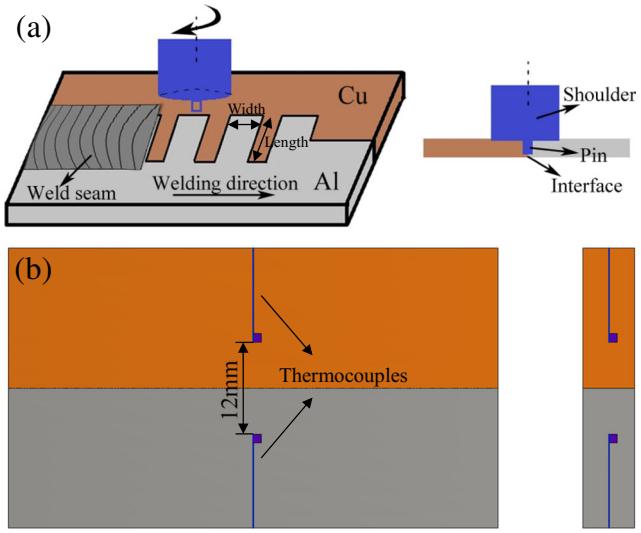

Fig. 1 Schematic illustrations of FSW setup. **a** Tooth-shaped joint configuration. **b** Position of the thermocouples

The relevant results were analyzed by comparing with the weld obtained via routine butting joint configuration (BJC) with the same processing parameters.

2 Experimental procedure

The base materials used were 1060 aluminum rolled plate and commercial pure copper with the thickness of 4 mm. Table 1 gives the elemental composition of base metals. Prior to welding, the plates were cleaned with acetone to remove the impurities and then placed on the backing plate rigidly. Experiments were accomplished in the vertical milling machine. The nonconsumable tool is composed of a shoulder (24 mm diameter) and a tapered pin, of which the diameter varies from 4 to 5 mm. The welding tool is plunged into the plates from the center location between the base metals and then moved along the welding line. Optimization experiments were implemented to obtain major machine variables in advance, including rotation speed 1500 rpm, traverse speed 30 mm/min, and plunging depth −0.2 mm, respectively. In addition, to strengthen the forging action of the shoulder, a 2° tilt angle was also adopted with respect to the vertical direction. Given the fact that Al has better flowability and filling ability, so controlling the weld composition with Al-rich content is a necessary measure to fabricate the defect-free weld. To achieve this purpose, the width of Al teeth was larger

Table 1 Chemical compositions of base metals (wt%)

	Al	Cu	Si	Zn	Fe	Ni	Pb
Al 1060	Bal.	0.005	0.07	0.005	0.30	0.0005	0.003
T2 Cu	0.02	Bal.	0.0069	0.69	0.05	0.03	0.03

than that of Cu teeth. Moreover, teeth length is a little shorter than the top diameter of the pin to ensure all the Al/Cu faying surface could be plasticized and then stirred into the bead during the welding.

Fabricating temperature plays a vital role in the microstructure evolution of the weld. Considering that the welding parameters keep constant, so temperature variation should be similar for the two joint configurations (BJC and TJC) and thermal profile was only recorded under BJC weld. Two K-type thermocouples were embedded at the middle-plate thickness (6 mm away from the butt line) of Al and Cu plates, respectively, to monitor the temperature history and Fig. 1b shows the scheme of the thermocouple site. Samples, extracted from the joint vertical to the welding direction, were subjected to mechanical grinding and polishing. And then, microstructure of the samples was investigated using optical microscopy (OM). Scanning electron microscopy (SEM), complemented by energy dispersive spectrum (EDS), was utilized to study the delicate microstructure and interfacial diffusion. X-ray diffraction (XRD) was applied to characterize the different phases. Tensile tests were performed to assess the weldment quality and tensile coupons were machined through the standard procedure. In order to exhibit the availability and repeatability of the process condition, the test was run through three specimens under the specific process condition. Finally, the fracture surface was examined and addressed carefully.

3 Results and discussion

3.1 Weld thermal history

In FSW, interfacial diffusion and microstructure evolution are thermally activated. Hence, it is very important to investigate the welding temperature carefully. Heat input is composed of two sources: one is the frictional heat generated between the rotating tool and workpiece and the other is the plastic deformation heat. The frictional heat takes up a large part. Al/Cu FSW will cause the asymmetric temperature distribution with respect to the adjoining surface because of the different property, which contributes to greater effect on the temperature field than different shearing rate and cannot be ignored. Consequently, two thermocouples were placed on Al and Cu sides, respectively, with the same distance from the interface to monitor the real-time temperature as illustrated in Fig. 1b. Previous studies have confirmed that the material on AS undergoes higher weld temperature than that on RS [21, 25].

Relationship between the temperature variation and time was highlighted in Fig. 2. Clearly, temperature curves are distinct on Al and Cu sides. Peak temperature of Cu side is about 60 °C higher than that on Al side. In addition, faster cooling rate was captured on Cu side, which could be ascribed to the fact that the high thermal conductivity ability of Cu led

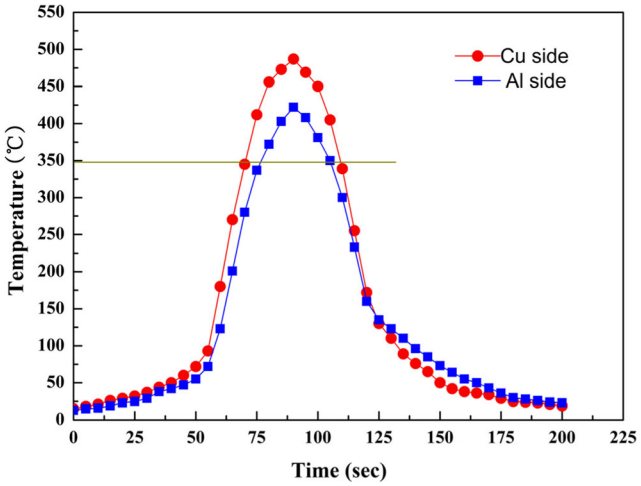

Fig. 2 Temperature profile measured on Cu and Al sides under BJC. Note: the horizontal line represents the temperature at 350 °C

to fast heat dissipation. The maximum temperature reached to 496 °C, which was lower than the Al/Cu eutectic point (548 °C), suggesting no melting occurred. Researchers [26] also found temperature varied little (lower than 20 °C) in the vertical direction of the workpiece. In the present case, temperature gap should be smaller between the top surface and mid-thickness plane of the plate because the thickness of the welded metals is 4 mm, thinner than that used in the reference. Under this circumstance, measured peak temperature could be treated as the maximum temperature the weld experienced. Meanwhile, holding time above 350 °C is short about 50 s, guaranteeing a short exposure to the high temperature, which could be indicated by the horizontal line marked in Fig. 2. There is no doubt that short heat exposure is helpful to suppress the thickening of diffusion layer.

3.2 Microstructure of the composite joints

The cross section of the joint synthesized with BJC was shown in Fig. 3a. Obviously, plasticized Cu fragment was dragged towards the other side and mixed with the deformed Al under the shoulder affected zone (SAZ) where a large amount of friction heat was produced accompanied by the strong stirring behavior of the shoulder. Figure 3b shows the enlarged image of region (b) in (a) and shattered Cu pieces are visibly appreciable due to the synergistic effect of the frictional heat and mechanical breakup. Based on Fig. 3c, high magnification of domain (c) in (a), Cu fragment was dragged towards Al side at the upper middle thickness and no material mixing occurred in the Al/Cu interface. Figure 3d shows the enlarged micrograph of the localized region (d) in (a) where alternate lamellae are captured and scratched Cu pieces, which were stirred into Al matrix, gave rise to the formation of this structure. Remarkably, the same structure was seldom detected in other region of the stir zone mainly due to lack of

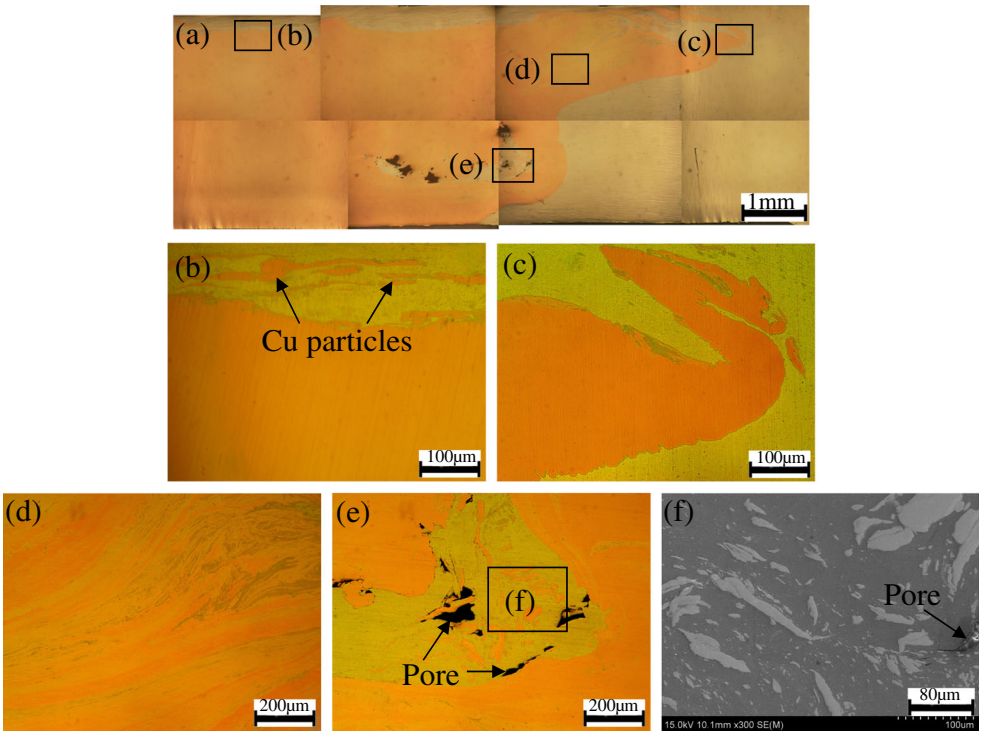

Fig. 3 Macro- and micrographs of the joint adopting BJC. **a** Macroscopy of the joint. **b** Enlargement of **b** in **a**. **c** Enlargement of **c** in **a**. **d** Enlargement of **d** in **a**. **e** Enlargement of **e** in **a**. **f** Enlargement of **f** in **e**

sufficient material mixing. Peeling role of the tool pin contributed to various Cu particles in the local region of the stir zone as indicated in Fig. 3e, which is the magnified view of region (e) in (a). However, void defects are also observed. In comparison with the upper part of the weld, low heat input resulted in the weak material softening and adversely affected the material flow. As a result, the extruded space cannot be filled completely, forming the pore defect. In Fig. 3f, enlargement of (f) marked in (e), various Cu particles were buried in the Al matrix and void defect is detectable.

Figure 4a presents the cross-section illustration of the defect-free joint with TJC. The advantage of this special joint design could be explained this way: when the tool advanced forward, alternate structure of base metals benefits the material mixing in the weld, and meantime more deformed Al with good flowability was also involved to fill the extruded space fully. Similar to the condition in Fig. 3a, Cu piece also stretched towards Al side owing to the shear stress of the plasticized material as shown in Fig. 4a. Obvious band structure was evidenced and the intercalated layer almost stretched in the same direction, which is closely associated with the fluid-like flow characteristic because of the movement of the tool as shown in Fig. 4b. Clearly, the new band was the resultant product of Al/Cu mixing and similar phenomenon has been reported [8]. Figure 4c is the enlarged micrograph of domain (c) in (a) and irregular Cu particles with various shape and size, which scattered on the Al matrix, were captured owing to the strong stir force of the tool pin. Figure 4d reveals the delicate view of the rectangle domain marked in (c) where particle rich zone (PRZ) was noticed with high-density particles and formed the Al matrix composite structure owing to the strong peeling effect of the tool with this special joint design. Besides, there is no pore or other defects in the weld, manifesting good fill ability of the soften material. EDS quantitative analysis was implemented through the localized region marked in Fig. 4d, and the result illustrated that diffusion has occurred and some particles, consisting of Al and Cu elements, may form the Al/Cu compound as highlighted in Fig. 4e. There is no doubt that the interfacial integrity could transfer external load from the matrix to strong particles efficiently. In conclusion, TJC favors the material mixing and element diffusion, which is beneficial to the joint performance.

3.3 Material flow

As stated before, alternate arrangement of base metals with TJC could facilitate material mixing. Compared with BJC, it is easier to produce Cu pieces with various sizes due to the insertion of Al. In addition, TJC also resulted in complex and turbulent flow characteristic, while material flow was obvious merely under the SAZ for BJC. Delicate flow behavior of TJC weld was analyzed. Figure 5a, enlargement of region A in Fig. 4a, shows the flow of Cu stripes towards Al side following the motion of the tool under the SAZ where high welding temperature facilitates the migration process with the aid of mechanical force. Apart from it, material flow was characterized by laminar pattern as shown in Fig. 5b, high magnification of region B in Fig. 4a. Apparently, the shear

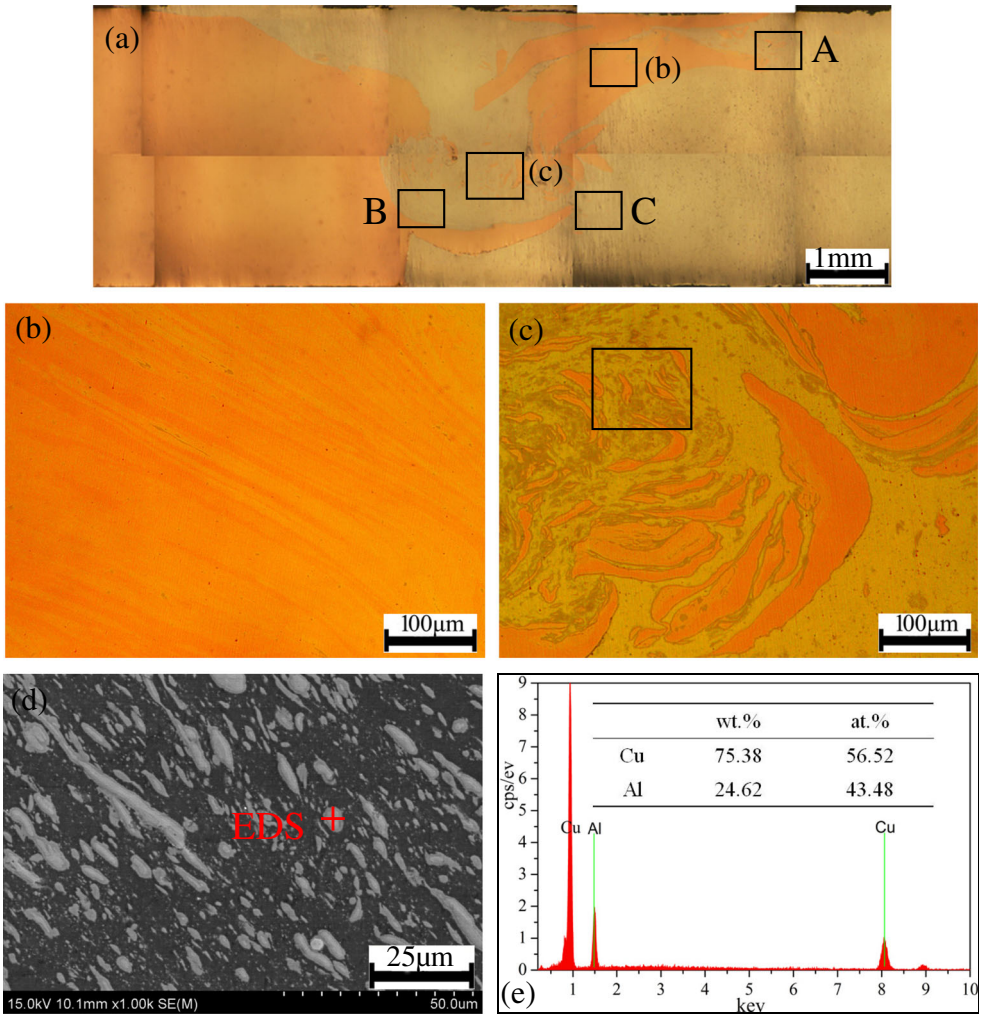

Fig. 4 Macro- and micrographs of the joint adopting TJC. **a** Macroscopy of the joint. **b** Enlargement of **b** in **a**. **c** Enlargement of **c** in **a**. **d** Enlargement of rectangle in **c**. **e** EDS result of the marked region in **d**

strain of plasticized material caused the material movement and produced the laminar feature. Dissimilar material flow usually produced complex, vortex-like patterns due to the different material properties. Figure 5c, enlargement of region C in Fig. 4a, represents the onion ring structure filled with irregular Cu-rich particles, which could be attributed to the reason that the deformed material is subjected to the entrainment role of the rotation and moving behavior of the pin where Al and Cu mixed with each other violently and produced the swirl-like flow feature. SEM images of Fig. 5b, c

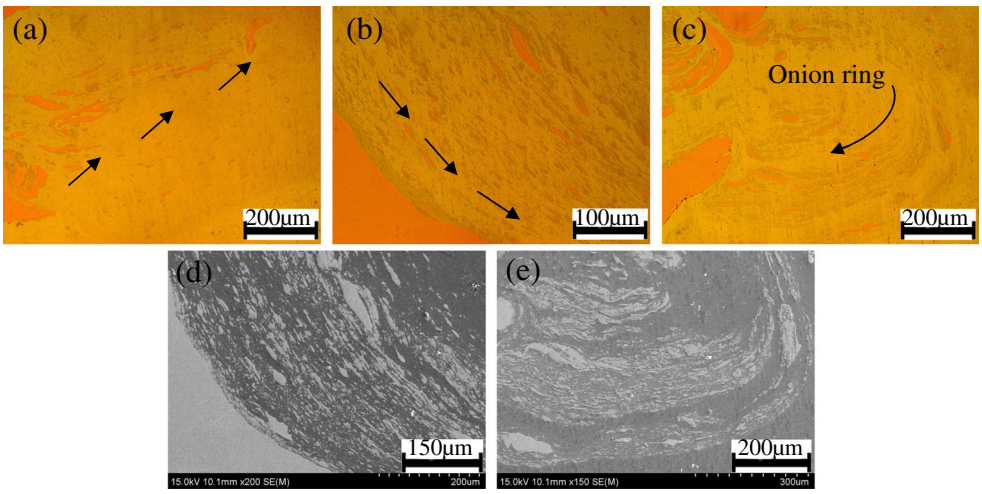

Fig. 5 Material flow behavior under TJC. **a** Enlargement of A in Fig. 4a. **b** Enlargement of B marked in Fig. 4a. **c** Enlargement of C marked in Fig. 4a. **d** SEM image of **b**. **e** SEM image of **c**

reveal the PRZ with high particle density as shown in subpanels d and e Fig. 5, respectively, manifesting a large volume of bulk Cu was plasticized, peeled, and mixed with Al. In other words, the insertion of Al tooth in the weld changed the sticking condition of deformed Cu and made it easier to break from the matrix in comparison with BJC, which is consistent with the microstructure analysis as well. As a consequence, enough evidence indicates that TJC has special advantage over BJC in improving the material mixing and flow.

3.4 Elemental diffusion behavior

For one thing, the interfacial diffusion layer is conductive to the weld performance due to the formation of metallurgical bonding. For another, in terms of the hard and brittle nature of Al/Cu intermetallic compounds (IMCs), the thick interlayer will exert deleterious effect on the adhesive strength of the joint unavoidably because cracks tend to initiate and propagate through it. A thin thickness, however, favors the weld strength and Xue et al. [27] investigated the Al/Cu butt welding and found the 2.5-μm diffusion thickness is the best for the ultimate tensile strength. Accordingly, it is important to characterize the interlayer. Figure 6a displays the SEM micrograph of the Al/Cu interface under BJC, and according to Fig. 6b, enlargement of (b) in (a), a clean interlayer without any defects was observed and it was composed of two sublayers, which could be interpreted this way: based on the diffusion principle, Al and Cu atoms migrate towards the opposite sides because of the concentration gradient. Then, Cu-rich and Al-rich compounds are prone to be formed preferentially near the matrix, so two different sublayers were created. Figure 6c gives the micrograph of the bond interface applying TJC and dispersed particles were detectable adjoining the interface, which differs from the circumstance shown in Fig. 6a. Again, the special

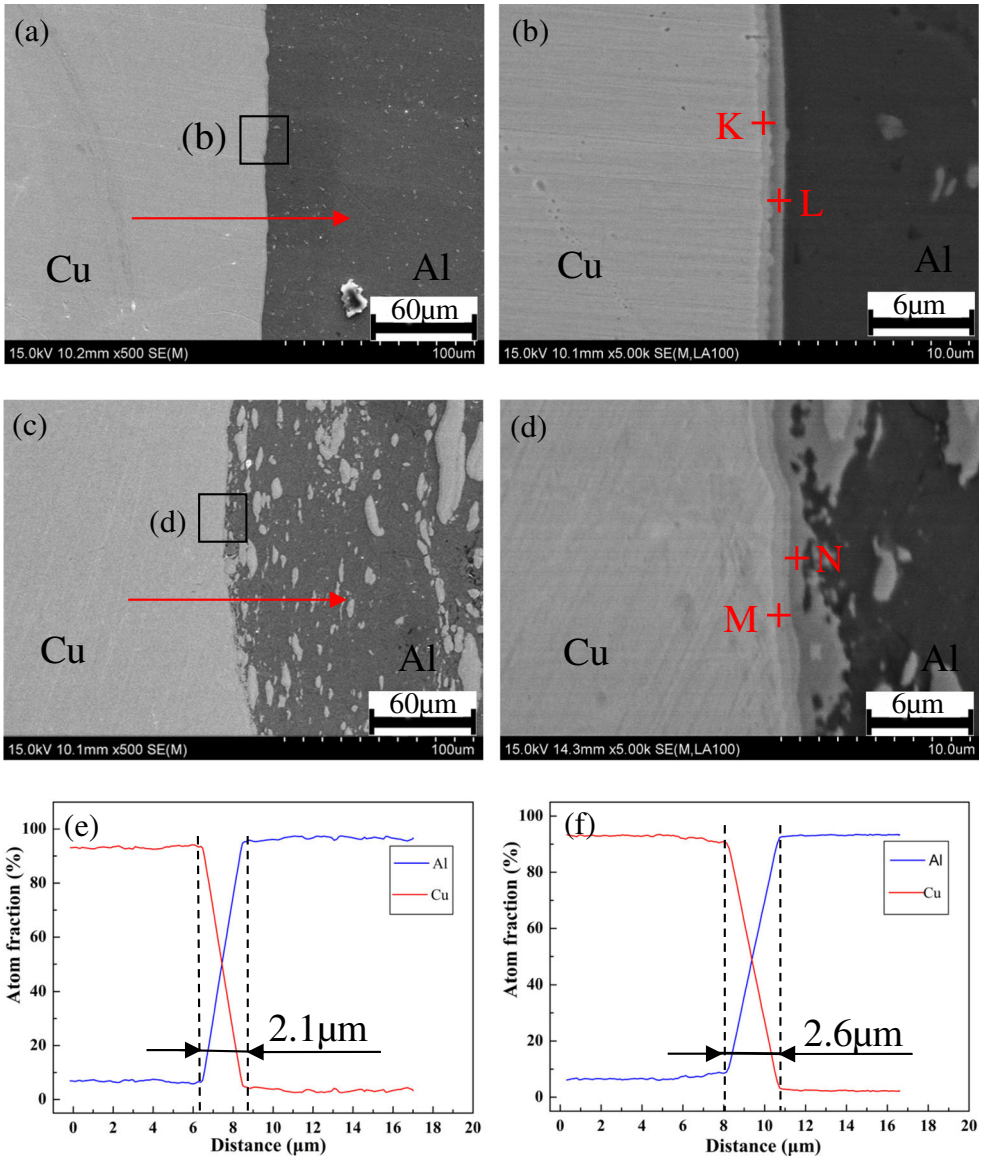

Fig. 6 Diffusion behavior of Al/Cu interface. **a** Micrograph of the interface with BJC. **b** Magnified view of **b** in **a**. **c** Micrograph of the interface with TJC. **d** Magnified view of **d** in **c**. **e** EDS line scan result in **a**. **f** EDS line scan result in **c**

advantage of TJC in scraping and scattering Cu pieces was exhibited. Similar to the condition in Fig. 6b, two flawless sublayers could also be observed as shown in Fig. 6d, high magnification of region (d) in (c). Elemental composition of the sublayers was detected utilizing EDS through regions K-N as marked in Fig. 6b and Fig. 6d, respectively. EDS through regions K and L marked in Fig. 6b and M and N marked in Fig. 6d, respectively. As shown in Table 2, Al content in region L (near the Al side) is twice higher than that in region K (near the Cu side), and likewise, high Cu content (60.08 atom fraction %) was detected in region K. The similar results were also obtained in regions M and N for TJC weld, which is also conformed to the concentration principle of elemental diffusion. It seems that two kinds of Al/Cu intermetallics were formed in the two sublayers, respectively. Corresponding constituent of the sublayer is nearly identical for the TJC weld and BJC weld due to the same welding parameters. Additionally, EDS line scan was implemented from Cu side to Al side as presented with the red-arrowed line in Fig. 6a, c. The line scan results were manifested in Fig. 6e, f, respectively. Obviously, both the interlayers are very thin (2.1 and 2.6 μm). As stated before, TJC contributes to the better material mixing, which favors the elemental diffusion, so the interlayer is a little thicker than that formed with BJC. Based on the kinetic mechanism of the dissimilar solid state welding, the formation of IMCs could be divided into three stages, namely, preparation, nucleation, and growth and reliable bonding could be produced during preparation stage [28]. The thickness and preparation stage of IMCs can be depicted by the equations as expressed below:

$$tH = t0\exp\left(\frac{Q}{RT}\right) \tag{1}$$

$$\delta^2 = Kt - tH \tag{2}$$

$$K = 9.1 \times 10^5 \exp\left(-\frac{100}{RT}\right) \tag{3}$$

where t_H and t_0 refer to the preparation time and the time of crystal nucleus starting to form, respectively. Q is the activation energy. R and T are representative of gas constant and heating temperature, respectively. δ refers to the interlayer thickness. K and t are constant and heating time, separately. Clearly, thickness δ has a positive correlation with the welding temperature T and holding time t. The thin interlayer thickness also accords with the measured temperature history in this investigation, namely, low peak temperature and short holding time as presented in Fig. 2.

Table 2 EDS results of regions K-N marked in Fig. 6b, d (atom fraction %)

Element	K	L	M	N
Cu	60.08	34.23	63.07	30.38
Al	39.92	65.77	36.93	69.62

Table 3 Activation energy of various Al/Cu IMCs

IMCs	AlCu	Al_2Cu	Al_3Cu_4	Al_2Cu_3	Al_4Cu_9
Activation energy (KJ/mol)	148.53	127.61	230.54	138.07	135.98

3.5 IMCs

According to the Al/Cu binary equilibrium phase diagram [29], Al and Cu could form limited solid solution at room temperature. In addition, five kinds of thermodynamically stable IMCs, including $Al_2Cu(\theta)$, $AlCu(\eta)$, $Al_2Cu_3(\delta)$, $Al_3Cu_4(\zeta)$, and $Al_4Cu_9(\gamma)$, could be developed during the thermal processing and Table 3 listed the activation energy of different intermetallics. As the occurrence of IMCs plays a vital role in the weld quality, XRD was conducted through the cross section of the joints to evaluate the phase composition of BJC and TJC joint, respectively. Figure 7 presented the XRD patterns. Al_2Cu and Al_4Cu_9 with low activation energy were formed for both the joints and the newly formed phases confirmed metallurgical bonding was achieved between base metals. Moreover, the result is also in agreement with the conclusion that Al_2Cu and Al_4Cu_9 are the first two formed IMCs during Al/Cu dissimilar FSW drawn by the researchers [30]. Noticeably, the peak intensity of the IMCs is weak, suggesting the low content, which is favorable for the mechanical property of the joint. Since the formation process of IMCs is thermally activated, the small amount of IMCs could be ascribed to the low peak temperature and short exposure to the thermal environment.

3.6 Mechanical property of the joint

Joint strength was evaluated by the tensile test and configuration of the tensile specimen obtained from the comparative experiments was shown in subpanels a and b of

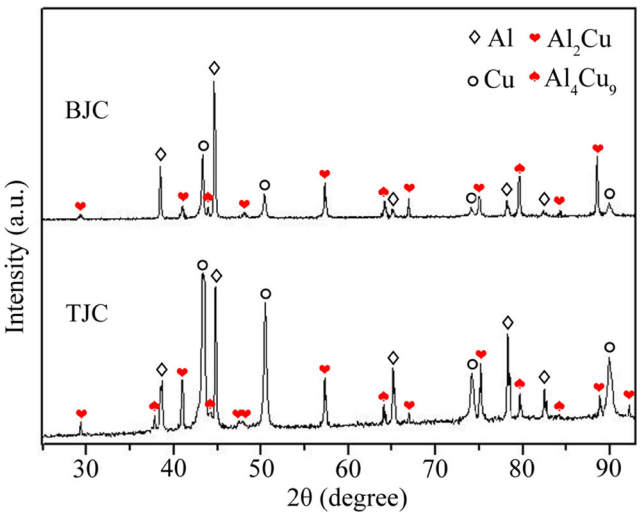

Fig. 7 XRD spectrums detected from the cross section of the joints

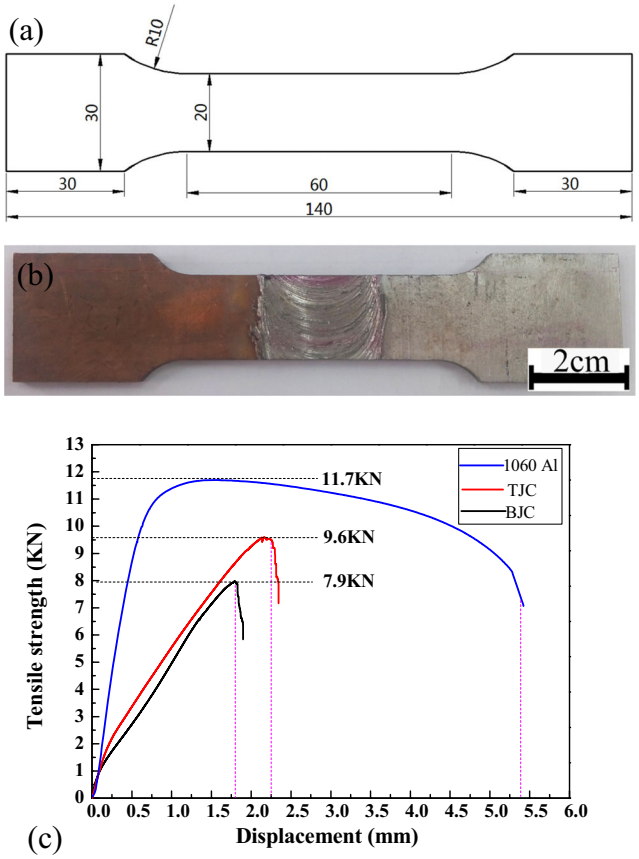

Fig. 8 Tensile test. **a** Scheme of the tensile coupon. **b** Physical photo of the tensile coupon. **c** Strength-displacement curves of the base metal Al and the joint under BJC and TJC, respectively

Table 4 EDS results of regions P-R marked in Fig. 9b, d (atom fraction %)

Element	P	Q	R
Al	98.13	77.81	86.27
Cu	1.87	22.19	13.73

Fig. 8, respectively. As a comparison, the tensile test of the base material Al was also implemented and Fig. 8c reveals the strength-displacement curve of the tensile specimens. Failure load of Al is about 11.7 kN and the large tensile displacement shows the good ductility to bear the deformation. With the improvement of the displacement, tensile load also increases continuously. For the weld, when the external force increased to the maximum value, the load decreased obviously with the slight improvement of the displacement. Clearly, the weld ductility is poor in comparison with the base metal, which is due to the occurrence of the welding stress and brittle intermetallics. The fracture strength of the BJC weld is 7.9 kN, which is about 67% of the base metal Al, with the tensile displacement 1.8 mm, while the tensile strength of the TJC weld reaches 9.6 kN, which is 80% of the base metal Al, without sacrificing the joint ductility (2.2 mm displacement). The tensile test validated the potential of TJC in enhancing the joint strength without losing the ductility.

Fractographic examination of the broken tensile specimens on Al side was carried out, and Fig. 9 presents the micrographs of the fracture morphology. Despite the fact

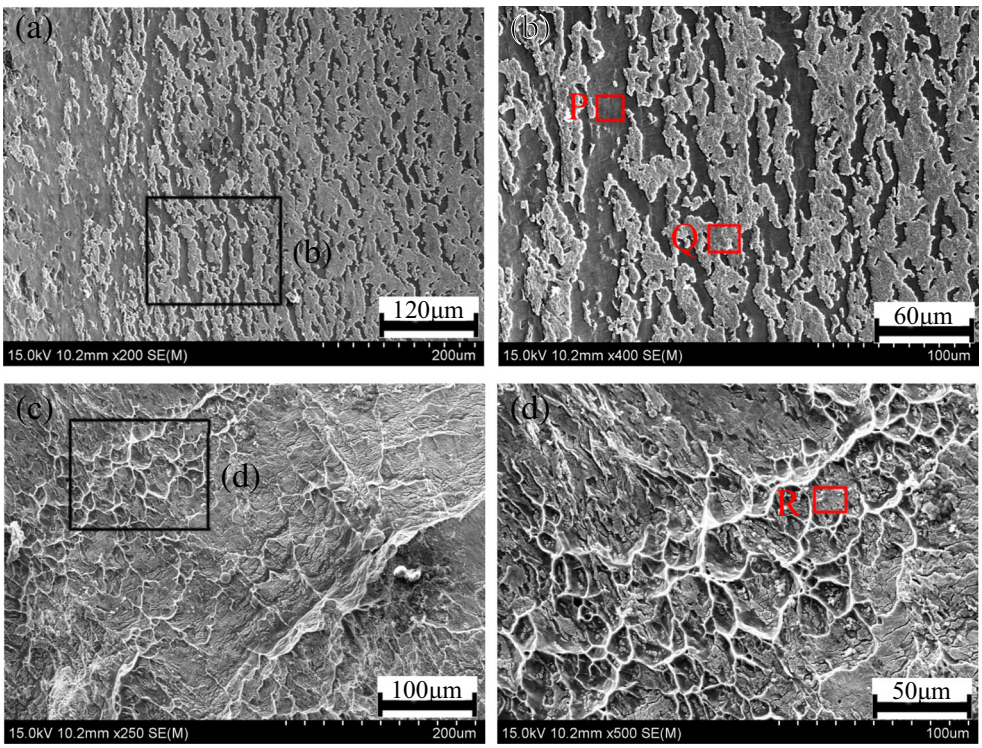

Fig. 9 The fractography examination on the Al side after tensile test. **a** SEM image of the fracture morphology with BJC. **b** Magnified view of **b** in **a**. **c** SEM image of the fracture morphology with TJC. **d** Magnified view of **d** in **c**

that the joints were processed under the same parameters for the comparative experiments, fracture appearance was characterized by distinctly different features.

Figure 9a highlights the fracture morphology of BJC weld, which is distinguished by the even surface, suggesting the brittle failure peculiarity. Obviously, the failure surface consists of two different parts, namely, light region and black background. The former takes up a large percent while the latter takes up a small part as shown in Fig. 9b, enlargement of region (b) in (a). EDS quantitative analysis of domain P and Q was revealed in Table 4. Al takes up 98.13% (atom fraction) for domain P and the black background is Al matrix, while the light part (region Q) is Al/Cu compound with 22% Cu content. Al/Cu compounds displayed high brittleness where crack initiation is likely to lie in and propagate. Consequently, the failure mechanism is the brittle fracture with small deformation for BJC weld. Nevertheless, the failure appearance was roughened with various dimples, indicating good fracture ductility for TJC weld. The dimple derived from the microvoid coalescence mechanism and the accumulated strain finally led to the failure during loading. Meantime, the dimple with various size is the representative of inhomogeneous deformation degree. Figure 9d, magnified view of domain (d) in (c), revealed the delicate fracture surface, which was separated by the ductile tearing edge. To some degree, the tearing edge shows that the joint could absorb the deformation and benefits the weld ductility. EDS quantitative analysis was conducted in domain R as marked in Fig. 9d, and the result was shown in Table 4. The elemental composition consists of 86.27% Al and 13.73% Cu (atom fraction), which confirms the occurrence of intense Al/Cu mixing. The high Al content may transform the fracture mode to ductile failure mechanism. From the perspective of microstructure, TJC is in favor of the joint ductility.

4 Conclusion

A set of comparative researches was carried out to explore the special advantages of TJC over the routine BJC in dissimilar Al/Cu friction stir welding. Based on the analysis in this paper, the following conclusions could be reached:

1. The welding temperature on Cu side (AS) was about 60 °C higher than that on Al side (RS) but much lower than Al/Cu eutectic melting. Additionally, the short holding time is also beneficial to hindering the development of brittle intermetallics.
2. Microstructure analysis showed the original joint design (TJC) enhanced material mixing and dispersive Cu particles in Al matrix produced the composite-like structure, while void defect was detected in the BJC weld.
3. XRD patterns revealed Al_2Cu and Al_4Cu_9 are the common IMCs developed under both the comparative experiments owing to the same hot working parameters.
4. Tensile strength is about 9.6 kN for TJC weld while it is 7.9 kN under BJC, and meanwhile the improvement of failure load did not sacrifice the weld ductility, highlighting TJC is a feasible design to enhance the mechanical property of the joint.
5. Fracture morphology of the broken specimen machined via TJC revealed ductile fracture characteristic, while brittle fracture mode appeared for BJC weld.

Acknowledgements The study work of this paper is supported by the National Natural Science Foundation of China (Grant No. 51475232).

This is a project funded by the Priority Academic Program Development of Jiangsu Higher Education Institutions (PAPD).

This is a project funded by the Foundation of Graduate Innovation Center in NUAA and the Fundamental Research Funds for the Central Universities (No. kfjj20160603).

References

1. Dorbane A, Ayoub G, Mansoor B, Hamade RF, Kridli G, Shabadi R, Imad A (2016) Microstructural observations and tensile fracture behavior of FSW twin roll cast AZ31 Mg sheets. Mater Sci Eng A 649:190–200
2. Sharma G, Dwivedi DK (2017) Study on microstructure and mechanical properties of dissimilar steel joint developed using friction stir welding. Int J Adv Manu Technol 88:1299–1307
3. Xue MS, Xie J, Li W, Ou JF, Wang FJ, Zhong ZC (2012) Characterization of interfacial strength of dissimilar metallic joints using a scanning Kelvin probe. Scr Mater 66(5):265–268
4. Yan ZJ, Liu XS, Fang HY (2016) Effect of sheet configuration on microstructure and mechanical behaviors of dissimilar Al–Mg–Si/Al–Zn–Mg aluminum alloys friction stir welding joints. J Mater Sci Technol 32(12):1378–1385
5. Mehta KP, Badheka VJ (2015) Influence of tool design and process parameters on dissimilar friction stir welding of copper to AA6061-T651 joints. Int J Adv Manu Technol 80(9):2073–2082
6. DebRoy T, Bhadeshia HKDH (2010) Friction stir welding of dissimilar alloys—a perspective. Sci Technol Weld Joi 15(4):266–270
7. Mishra RS, Ma ZY (2005) Friction stir welding and processing
8. Tan CW, Jiang ZG, Li LQ, Chen YB, Chen XY (2013) Microstructural evolution and mechanical properties of dissimilar Al–Cu joints produced by friction stir welding. Mater Des 51:466–473
9. Zhao Y, Jiang S, Yang SF, Lu ZP, Yan K (2016) Influence of cooling conditions on joint properties and microstructures of aluminum and magnesium dissimilar alloys by friction stir welding. Int J Adv Manu Technol 83(1):673–679
10. Dorbane A, Mansoor B, Ayoub G, Shunmugasamy VC, Imad A (2015) Mechanical, microstructural and fracture properties of dissimilar welds produced by friction stir welding of AZ31B and Al6061. Mater Sci Eng A 170:251–260
11. Somasekharan AC, Murr LE (2004) Microstructures in friction-stir welded dissimilar magnesium alloys and magnesium alloys to 6061-T6 aluminum alloy. Mater Charact 52(1):49–64
12. Rafiei R, Moghaddam AO, Hatami MR, Khodabakhshi F, Abdolahzadeh A, Shokuhfar A (2017) Microstructural

characteristics and mechanical properties of the dissimilar friction-stir butt welds between an Al–Mg alloy and A316L stainless steel. Int J Adv Manu Technol 90(9–12):2785–2801
13. Zheng QX, Feng XM, Shen YF, Huang GQ, Zhao PC (2016) Dissimilar friction stir welding of 6061 Al to 316 stainless steel using Zn as a filler metal. J Alloy Compd 686:693–701
14. Ramachandran KK, Murugan N, Kumar SS (2016) Performance analysis of dissimilar friction stir welded aluminium alloy AA5052 and HSLA steel butt joints using response surface method. Int J Adv Manu Technol 86:2373–2392
15. Zebardast M, Karimi Taheri A (2011) The cold welding of copper to aluminum using equal channel angular extrusion (ECAE) process. J Mater Process Technol 211(6):1034–1043
16. Sahu PK, Pal S, Pal SK, Jain R (2016) Influence of plate position, tool offset and tool rotational speed on mechanical properties and microstructures of dissimilar Al/Cu friction stir welding joints. J Mater Process Technol 235:55–67
17. Galvão I, Leal RM, Loureiro A, Rodrigues DM (2010) Material flow in heterogeneous friction stir welding of aluminium and copper thin sheets. Sci Technol Weld Joi 15: 654–660
18. Xue P, Ni DR, Wang D, Xiao BL, Ma ZY (2011) Effect of friction stir welding parameters on the microstructure and mechanical properties of the dissimilar Al–Cu joints. Mater Sci Eng A 528(13): 4683–4689
19. Carlone P, Astarita A, Palazzo CS, Paradiso V, Squillace A (2015) Microstructural aspects in Al–Cu dissimilar joining by FSW. Int J Adv Manu Technol 79(5):1109–1116
20. Al-Roubaiy AO, Nabat SM, Batako ADL (2014) Experimental and theoretical analysis of friction stir welding of Al–Cu joints. Int J Adv Manu Technol 71(9):1631–1642
21. Liu HJ, Shen JJ, Zhou L, Zhao YQ, Liu C, Kuang LY (2013) Microstructural characterisation and mechanical properties of friction stir welded joints of aluminium alloy to copper. Sci Technol Weld Joi 16(1):92–98
22. Mehta KP, Badheka VJ (2016) Hybrid approaches of assisted heating and cooling for friction stir welding of copper to aluminum joints. J Mater Process Technol 239:336–345
23. Seidel TU, Reynolds AP (2011) Visualization of the material flow in AA2195 friction-stir welds using a marker insert technique. Metall Mater Trans A 32(11):2879–2884
24. Zhang W, Shen YF, Yan YF, Guo R (2017) Dissimilar friction stir welding of 6061 Al to T2 pure Cu adopting tooth-shaped joint configuration: microstructure and mechanical properties. Mater Sci Eng A 690:355–364
25. Jafarzadegan M, Abdollah-Zadeh A, Feng AH, Saeid T, Shen J, Assadi H (2013) Microstructure and mechanical properties of a dissimilar friction stir weld between austenitic stainless steel and low carbon steel. J Mater Sci Technol 29(4):367–372
26. Mahoney MW, Rhodes CG, Flintoff JG, Bingel WH, Spurling RA (1998) Properties of friction-stir-welded 7075 T651 aluminum. Metall Mater Trans A 29(7):1955–1964
27. Xue P, Xiao BL, Ma ZY (2015) Effect of interfacial microstructure evolution on mechanical properties and fracture behavior of friction stir-welded Al-Cu joints. Metall Mater Trans A 46:3091–3103
28. Shi CY, Yu QZ (2012) Welding of dissimilar metals. China Machine Press, Beijing
29. ASM handbooks. Vol. 3 (2002) Alloy phase diagrams. ASM International, Materials Park, OH
30. Genevois C, Girard M, Huneau B, Sauvage X, Racineux G (2011) Interfacial reaction during friction stir welding of Al and Cu. Metall Mater Trans A 42(8):2290–2295